Thermal Topology Optimization of a Three-Layer Laminated Busbar for Power Converters

Oriol Puigdellivol, Damien Méresse, Yvonnick Le Menach, Souad Harmand, and Jean-François Wecxsteen

***Abstract*—This paper focuses on a topology optimization method for laminated busbars in power converters that minimizes the quantity of copper used while keeping the temperature under the allowed limits. Busbars are widely studied for adding their stray inductance to the commutation loop, which causes surge voltage across the power devices. However, the study of heat dissipation is essential to control hotspots in the busbar and preserve the converter components. Current density and temperature are sensitive to shape modifications; hence, topology optimization based on multiphysics simulations is an aspect to be considered when designing prototypes for a good cost performance ratio. The temperature is calculated by an electrothermal two-dimensional (2-D) finite element method (FEM) superposition approach. Busbar plates are modeled in 2-D since the thickness is constant. Furthermore, the different layers are related by the thermal equations reproducing the heat transfers regarding the overlap in the laminated busbar. Simulation results are validated by experimental tests. Comparison with 3-D FEM proves the 2-D approach to be faster while remaining accurate and a perfect method for topology optimization resolutions, which are very time consuming for three-dimensional (3-D) geometries. The busbar topology optimization is made by maximizing the energy transfer with the environment and by varying the electric and thermal conductivities of the mesh elements. Optimization leads to more than 50% volume reduction.**

***Index Terms*—Busbar, converters, heat transfer, optimization, thermal management.**

I. Introduction

LAMINATED busbars interconnect the power switching devices to other electronic components in power converters. All the advantages compared to cable wiring reside on the geometry, while being flat, rigid, and compact, which allow mechanical support for the devices, weak stray inductance, and heat dissipation.

Manuscript received April 18, 2016; revised July 15, 2016; accepted August 2, 2016. Date of publication August 16, 2016; date of current version February 11, 2017. Recommended for publication by Associate Editor K. Ngo.

O. Puigdellivol is with the Laboratoire d Electrotechnique et d Electronique de Puissance (L2EP), Centrale Lille, Arts et Métiers Paris Tech, HEI, University of Lille, Lille F-59000, France. He is also with LAMIH UMR CNRS 8201, Université de Valenciennes et Hainaut-Cambrésis, Famars 59300, France, and with AUXEL FTG, Gondecourt FR-59147, France (e-mail: puigde.oriol@gmail.com).

D. Meresse and S. Harmand are with LAMIH UMR CNRS 8201, Université de Valenciennes et Hainaut-Cambrésis, F-59313 Valenciennes, France (e-mail: damien.meresse@univ-valenciennes.fr; souad.harmand@univ-valenciennes.fr).

Y. L. Menach is with the Laboratoire d Electrotechnique et d Electronique de Puissance (L2EP), Centrale Lille, Arts et Métiers Paris Tech, HEI, University of Lille, Lille F-59000, France (e-mail: yvonnick.le-menach@univ-lille1.fr).

J.-F. Wecxsteen is with AUXEL FTG, Gondecourt FR-59147, France (e-mail: jfw@auxel.com).

Color versions of one or more of the figures in this paper are available online at http://ieeexplore.ieee.org.

Digital Object Identifier 10.1109/TPEL.2016.2601010

The main purpose of busbars is to reduce stray inductance as during the turn-off transient of the switching power devices, voltage overshoot occurs. This peak, a result of high *di/dt* and stray inductance, increases losses and could lead to the module failure. The overshoot is directly related to the sum of inductances taking part in the commutation loop path such as the busbars, the capacitors, and the power modules. This topic is widely studied and several papers can be found in the literature. Techniques concerning inductance minimization are based on reducing the commutation loop size by rearranging the layers disposition [1], [6], [10], widening conductive sections [2], [7], and using the symmetry concept [5], [8].

Temperature cannot be ignored as it is a critical parameter for the design of busbars. Current density prediction across the busbar allows us to determine the creation of possible hotspots. These hotspots are the result of a thin section with high current density, and they increase the temperature significantly across the busbar. As the temperature increases, the electrical conductivity decreases, leading to higher Joule heating. Consequently, high temperatures can damage not only the adhesive used between conductors and dielectric films but also the semiconductor devices as manufacturers set temperature limits for the converter operations. An optimal conception must avoid these problems without forgetting that temperatures that are too low are a sign of oversized systems and waste of material. Temperatures must be calculated in steady state at the maximum converter power possible in order to set the worst-case scenario and not exceed the maximum allowed temperatures. The temperature variations from alternating current can be ignored as thermal transients are slower than the electric ones.

Regarding electromagnetic modeling, different numerical methods are used: the finite element method (FEM) and the partial element equivalent circuit (PEEC). The FEM method is generally used for precise results at the expense of computation time. The PEEC method extracts parasitic parameters: resistance and self- and mutual inductances from a volume discretized in elementary filaments forming an *RL* circuit. The PEEC method proves to be an alternative to the FEM as given in [3] and [10] since problem resolutions are quick but less accurate. For temperature calculations in busbars, multiple analytical methods can be found in the literature [4], [14]; however, these methods are limited to simplified geometries. Moreover, numerical tools such as FEM [15] or lumped parameter thermal model (LPTM) [16] are more precise and can be applied for complicated busbar geometries and also allow the temperature dependency of electrical parameters. To do so, a multiphysics looping between the electrical and thermal problems has to be performed during

the numerical resolution. Numerical three-dimensional (3-D) analysis can be applied, but the fact that insulating layers are less than 0.5 mm thickness significantly increases the unknowns of the problem and the calculation time; therefore, this method is limited for optimization. In Section II, a two-dimensional (2-D) numerical superposition method based on FEM is developed for modeling laminated busbars, taking advantage of the constant thickness of the conductive plates (temperature is considered constant inside the thickness). With this method, based on FEM, good accuracy is achieved, and by reducing the problem to two dimensions, the calculation time is significantly reduced. An electrothermal 2-D problem is solved in each plate of the laminated busbar and then interrelated with the other plates by the thermal equations. These thermal equations are consistent with the overlap of the plates in the assembly. In Section III, the 2-D method is compared and validated against experimental measures of a three-layer laminated busbar. In Section IV, a slightly different three-layer busbar is simulated under the operation conditions by 2-D approach and the 3-D FEM showing an oversized geometry. Comparison of the time to results between both approaches gives the 2-D superposition method an advantage to apply topology optimization without expensive time calculations. Optimization is done by considering the plate's thickness and shape in order to balance the temperature limits with the amount of material used.

About topology optimization in busbars and according to electromagnetic calculations, optimization of shape is also studied by [13] using the PEEC method and a genetic algorithm (AG) in order to minimize inductance and balance currents. Regarding thermal transfers, Matsumori *et al*. [17] propose a topology optimization for fluid and thermal interaction problems and Iga *et al*. [18] propose an optimization for thermal conductors considering conduction and convection. However, Hong [19] considers that the main power dissipation is removed by conduction.

In this paper (see Section V) and thanks to the fast resolutions of the 2-D superposition method, a thermal topology optimization is proposed so that electrothermal resolutions are performed along with an optimization algorithm. Volume reduction is accomplished first by reducing the thickness of the plates and then by doing a topology shape optimization. For the topology optimization, it is necessary to adapt the 2-D electrothermal FEM solver with a discrete mapping of the elements density, which changes the electric and thermal conductivities. This method is similar to the solid isotropic material with penalization (SIMP), which turns the density of the elements into a continuous variable [12]. The mapping density method consists of canceling both electrical and thermal conductivities of the targeted elements in the mesh, allowing the resolution of new shapes without remeshing. This method coupled with the optimization algorithm, which targets the elements to remove, turns into fast resolutions. The novelty of the paper resides in the adaptation of a 3-D problem into several 2-D problems without losing accuracy and allowing fast topology optimizations.

II. 2-D Superposition Method

The developed method consists in solving a 3-D multilayer busbar geometry by 2-D FEM-coupled problems (electric and thermal) (see Fig. 1). The objective of this method is to allow fast electrothermal resolutions for the subsequent application of a topology optimization in the different plates. To do so, each conductive plate is treated as a single 2-D problem. The resolution is done by an electrokinetic model followed by a thermal one. The different layers are then related by the thermal boundary conditions. These thermal boundary conditions are solved locally and depend on the relative position between the plates [see Fig 1(c)]. The general equations of both models are presented later to describe a general case for three conductive layers. Finally, the description of the procedure for the 2-D superposition method is detailed.

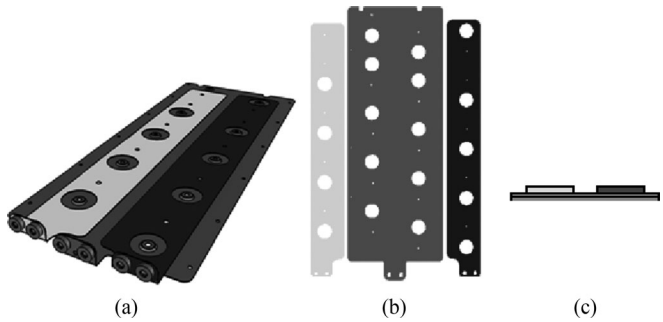

Fig. 1. (a) Three-dimensional busbar. (b) Two-dimensional conductive plates. (c) Section cut of the relative position between plates.

A. Electrokinetic Model

The first step of the method is the geometry definition of the conductive plates. With the aid of a numerical tool (MATLAB), simple images of the plates are used to upload the geometric shape into the solver. Then, the geometric shapes are meshed and solved by the electrokinetic model from the MATLAB PDE toolbox. The electric problem is solved by the following equation in all conductive plates:

$$\nabla \cdot \frac{1}{\rho} \cdot (-\nabla V) = \nabla J_S \tag{1}$$

where ρ is the resistivity and hence $1/\rho$ is the electrical conductivity, and J_S is the current source. Current inputs and outputs are modeled with Neumann boundary conditions defining the normal component of the current density, and the outer boundaries are set to 0 (isolated). The Joule heating is calculated by the resolution of the electric problem and used as heat source for the thermal problem

$$Q = \rho |J|^2 = \rho \left| \frac{1}{\rho} E \right|^2 = \frac{1}{\rho} |\nabla V|^2. \tag{2}$$

B. Thermal Model

Once the Joule heating is calculated, the thermal model is solved by the MATLAB'S PDE heat transfer problem. Considering the domain under study *D* a conductive plate (see Fig. 2), the thermal resolution depends on the possible heat transfers between D and its environment, which can be air or contact with other plates. Equation (3) stands for the thermal diffusion inside domain D with thermal conductivity λ and temperature

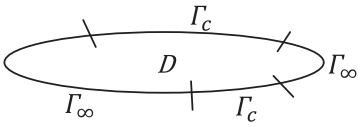

Fig. 2. Computational domain

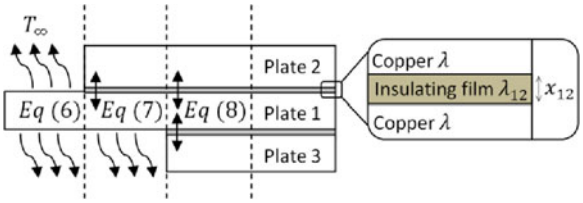

Fig. 3. Section cut of a three-layer laminated busbar. Plates are separated by an insulating film (gray) of x_{12} thickness, zoomed zone. The entire system is surrounded by air with the environment temperature T_∞. Curved arrows represent convection and radiation. Straight arrows stand for conduction.

T. The possible boundary conditions are defined by Γ_∞ and Γ_c. Γ_∞ (4) stands for convective and radiative transfer between *D* and the air at T_∞, where h is the convective coefficient, the surface emissivity is defined by ε and σ stands for the Boltzmann constant. Γ_c (5) represents the thermal conduction between *D* and another plate at temperature T_c through an insulating film of conductivity λ_i and thickness x_i

$$D \rightarrow \ -\nabla \cdot (\lambda \nabla T) \tag{3}$$

$$\Gamma_\infty \rightarrow \ h(T - T_\infty) + \varepsilon\sigma\left(T^4 - T_\infty^4\right) \tag{4}$$

$$\Gamma_c \rightarrow \ \frac{\lambda_i}{x_i}(T - T_c). \tag{5}$$

Fig. 3 illustrates the section cut of a three-layer laminated busbar and the three possible combinations of the boundary conditions (4) and (5). The resulting local thermal equations defining the problem are (6), (7), and (8)

$$-\nabla \cdot (\lambda \nabla T) + 2h(T - T_\infty) + 2\varepsilon\sigma\left(T^4 - T_\infty^4\right) = Q \tag{6}$$

$$-\nabla \cdot (\lambda \nabla T) + h(T - T_\infty) + \varepsilon\sigma\left(T^4 - T_\infty^4\right) + \frac{\lambda_{12}}{x_{12}}(T - T_2) = Q \tag{7}$$

$$-\nabla \cdot (\lambda \nabla T) + \frac{\lambda_{12}}{x_{12}}(T - T_2) + \frac{\lambda_{13}}{x_{13}}(T - T_3) = Q. \tag{8}$$

The first term of (6), (7), and (8) corresponds to the thermal diffusion, i.e., the domain under study (named plate 1 in Fig. 3). Convection and radiation terms are multiplied by 2 in (6) by considering that both sides of the domain are under Γ_∞ conditions. Equation (7) adds thermal conduction instead of a second term for convection and radiation so the domain is under Γ_∞ and Γ_c conditions. The insulating film placed between the plates (plates 1 and 2) has x_{12} thickness and λ_{12} thermal conductivity. T_2 represents the element temperature from *plate 2* standing in front of the element treated in the domain. Finally, in (8), the double thermal conduction Γ_c case, where conduction between the domain and *plates 2* and *3* occurs.

Once the thermal resolution is done, the electrical resistivity ρ is recalculated since it depends on the temperature. Therefore, a looping concerning the electrical and the thermal resolution is carried out until the convergence of the final temperature

$$\rho = \rho_0 \left[1 + \alpha \left(T - T_a\right)\right] \tag{9}$$

where ρ_0 is the resistivity at the ambient temperature T_a and α is the coefficient determining the variation of the resistivity with the temperature.

Fig. 4 shows the flowchart when using the 2-D superposition method for temperature calculations. In every electrothermal simulation, a loop (gray one) is performed to take into account the temperature dependency of the electric resistivity until the error between the previous temperature values and the current ones reach a defined value. The first resolution of the flowchart for all plates is simulated in a double convection–radiation state [plates surrounded by air (6)] in order to have an initial solution for all the plates. Consecutively, another loop (the left one) applies the appropriate thermal equation (6), (7), or (8) regarding the relative position between plates and updates the external plates temperatures [T_c in boundary conditions (5)], allowing the thermal conductive flow between them. The simulation reaches the final result when the errors between precedent temperatures of all plates and the current ones are less than a fixed value.

Using a well-adapted convective coefficient h becomes a critical decision for achieving accurate results. In this paper, only natural convection is treated. Warm air tends to rise, so depending on the spatial position of the plates, the natural convection coefficient varies significantly. Different correlation factors for different spatial dispositions allow calculating the convection coefficient [9]. These correlations are valid for laminar flow, which means a Grashof number (10) less than 10^9, where L is the characteristic length, δ the fluid density,g the gravitational acceleration, β the coefficient of thermal expansion, and μ is the kinematic viscosity. The possible spatial dispositions are the vertical plate (11) (where both surfaces are under same conditions), upper surface for the horizontal plate (12), and lower surface for the horizontal plate (13). These correlations depend on the characteristic length L of the plate and the gradient between the surface temperature and the ambiance T_∞. Since the applied method uses 2-D problems, the chosen coefficient is the mean value of both faces

$$\mathrm{G}r = \ \frac{L^3 \delta^2 g \beta \Delta T}{\mu^2} \tag{10}$$

$$h = \ 1.42\left(\frac{T - T_\infty}{L}\right)^{0.25} \tag{11}$$

$$h = \ 1.32\left(\frac{T - T_\infty}{L}\right)^{0.25} \tag{12}$$

$$h = \ 0.66\left(\frac{T - T_\infty}{L}\right)^{0.25}. \tag{13}$$

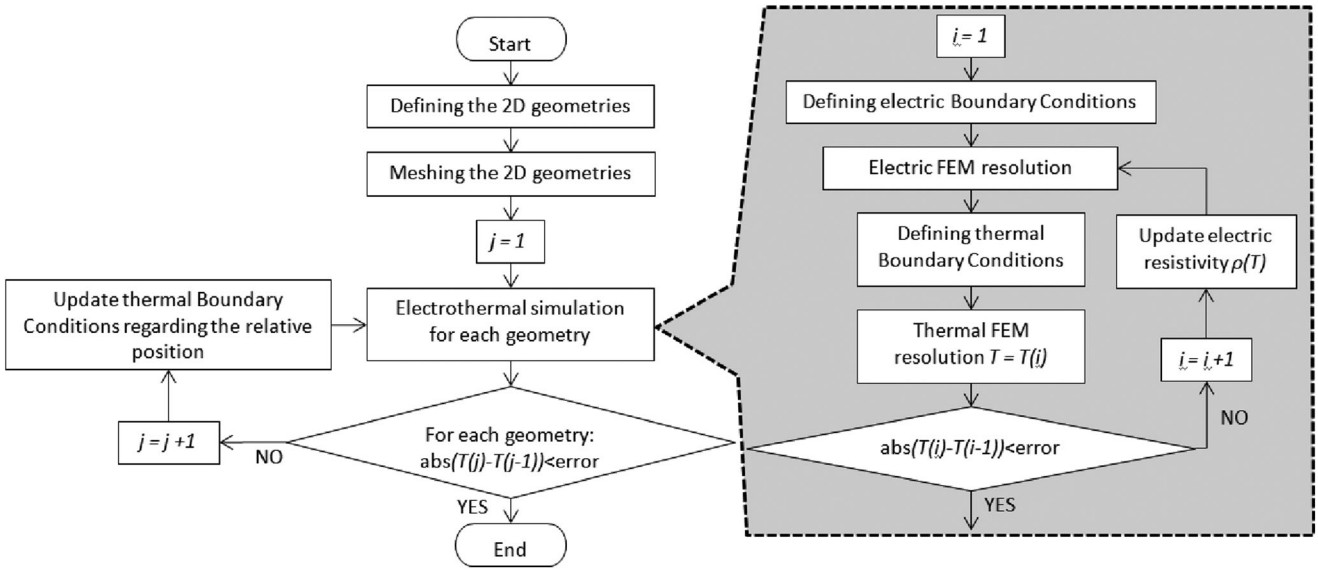

Fig. 4. Flowchart for determining the temperature of the laminated bubsar with the 2-D superposition method.

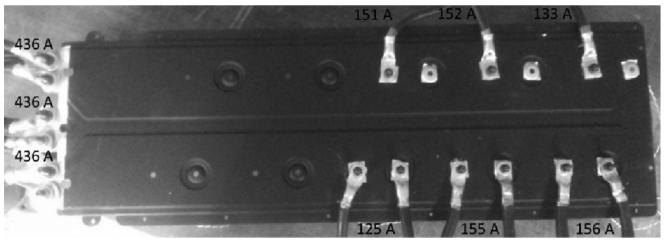

Fig. 5. Experimental setup of the busbar with the current connections.

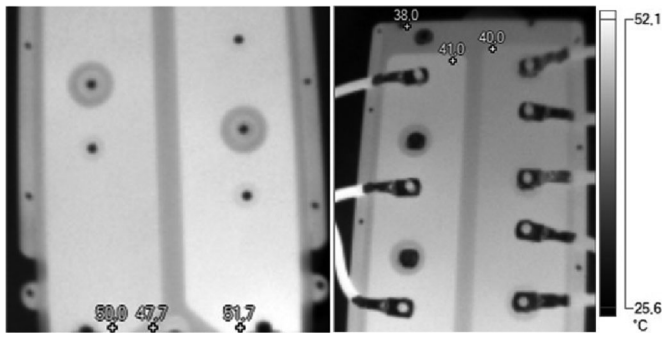

Fig. 6. Measures of the maximum and minimum temperature taken with the infrared camera.

III. Experimental Validation

A three-layer laminated busbar has been physically tested to validate the 2-D superposition method. The temperature has been measured with an infrared camera (Fluke Ti125) after painting the surface with black paint ($\varepsilon = 0.98$); the measures have an accuracy of ± 1 °C. The busbar has been connected to a generator, and the currents across the plates have been reproduced in the simulation according to the measures of current done in the experimental setup (see Fig. 5). The ambient temperature is 25 °C.

Measures have been taken in a thermal steady state after 100 min (see Fig. 6). The convection coefficient used in the simulation is the mean of (12) and (13). The thermal images have been overlapped and compared with the thermal simulation (see Fig. 7). The maximum error of temperature rise between measures and simulation over the plate's surfaces is below 9% (see Fig. 8). Error is higher in the edges and in the connections where the measure is not reliable. These results are accurate considering the simplifications adopted in the simulation where just the 2-D conductive plates are modeled without the connecting wires.

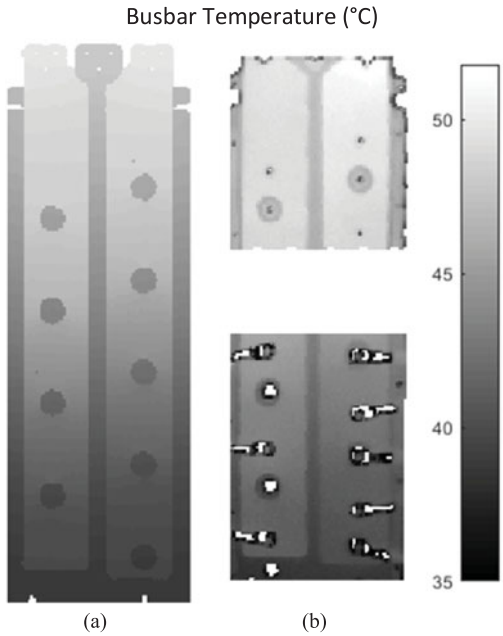

Fig. 7. (a) Simulated temperature. (b) Thermal images adapted to the busbar geometry.

IV. Simulation Results

Once the method is validated, another 3 layer laminated busbar (Fig. 9) is simulated at the operating conditions in order to

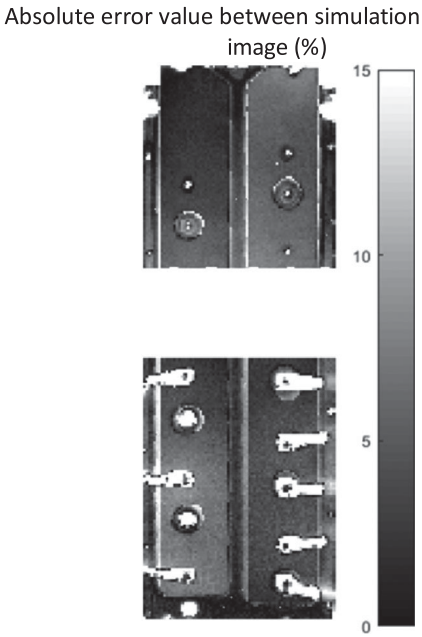

Fig. 8. Absolute error between the temperature simulated and the temperature measured.

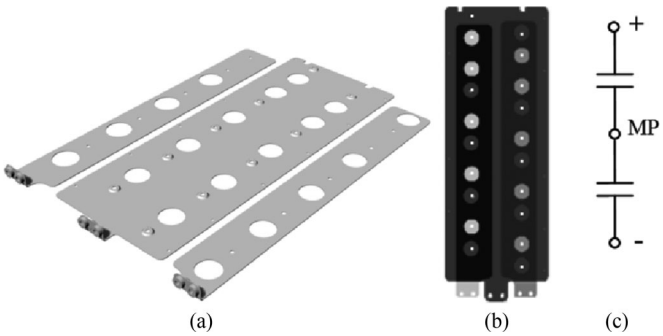

Fig. 9. (a) Exploded 3-D view of the three plates of the laminated busbar. (b) 2-D view of the simulated plates in superposition method. (c) Electric scheme with the positive potential (+), the MP, and the negative potential (−).

compare results and time saving between the 2-D superposition method and the 3-D FEM method. This simulation also allows seeing whether or not the busbar is oversized. This busbar is formed by three copper conductors of 1 mm thickness each. The big plate is for the medium dc-link potential (MP) while the other ones stand for the positive dc-link potential (+) and the negative dc-link potential (−). The whole system size is 236 × 672 mm. The busbar is intended for connecting the capacitor bank with an IGBT busbar. The 3-D FEM geometry is treated by pre- and postprocessing software, and the numerical resolution is performed by coupling an electromagnetic code and a thermal code. Two different current values are compared; the parameters used in the simulations are listed in Table I, with $A_{\rm eff} = 240$ being the real operation conditions for the busbar.

For the 2-D superposition method, the geometry simulated is shown in Fig. 9(b), while for the 3-D FEM simulation, a CAD file is used. The results from the simulations are shown in Table II. Comparing both simulation results, the difference between temperature rises is less than 6% (plate 3). According

TABLE I
INPUT PARAMETERS OF THE BUSBAR SIMULATION

Parameter	Value
Current $A_{\rm eff}$	240/350
Insulating film conductivity (W/m·K)	0.2373
Insulating film thickness (mm)	1.42
Emissivity	0.15
Average convection coefficient (W/m^2·K)	2.525
Ambient temperature (°C)	70

TABLE II
COMPARISON OF THE MAXIMUM TEMPERATURES FROM THE SIMULATION RESULTS

Current $A_{\rm eff}$	Plate	Temperature (°C)		ΔT Difference %
		2-D	3-D	
240	1 (+)	83.8	83.3	3.6
	2 (MP)	83.3	82.8	3.8
	3 (−)	84.7	83.9	5.4
350	1 (+)	94.9	94.22	2.7
	2 (MP)	93.49	93.17	1.4
	3 (−)	95.87	95.43	1.7

to the time to results, the 2-D superposition method represents an advantage since is faster. The time to results corresponds to the total time consumed considering the geometry definition, the meshing and the inputs definition, and the numerical resolution. With the 2-D superposition method, the time to results is of the order of 10 min, whereas the 3-D FEM stands for more than 100 min.

According to the temperature values in Table II, in particular, the 240A row which corresponds to the operating conditions for the busbar, the highest temperature is 84.7 °C (see Fig. 11 for the temperature distribution in the plates). The most restricting temperature of the system is the maximum temperature allowed by the glue used between the insulating films and conductors, which is 105 °C. In this case, the busbar system can be considered oversized, and it is possible to optimize it by reducing the conductors' volumes.

V. TOPOLOGY OPTIMIZATION

The objective of the topology optimization is to reduce the amount of copper used in the laminated busbar while targeting a maximum allowed temperature. This temperature cannot exceed the semiconductor device's temperature limit set by the manufacturer, normally 120 °C for the IGBTs, or the temperature limit of the adhesive used for fixing the insulating films, which withstands 105 °C at thermal steady state and 115 °C for peak temperatures. The 2-D superposition method is used for the thermal simulation because of the fast resolution time. Furthermore, it easily allows the implementation of topology optimization techniques such as thickness optimization and shape optimization.

First, optimization concerning the plate's thickness is applied in order to reach temperatures below the limit and save a large amount of copper, without modifying the original shape. Since

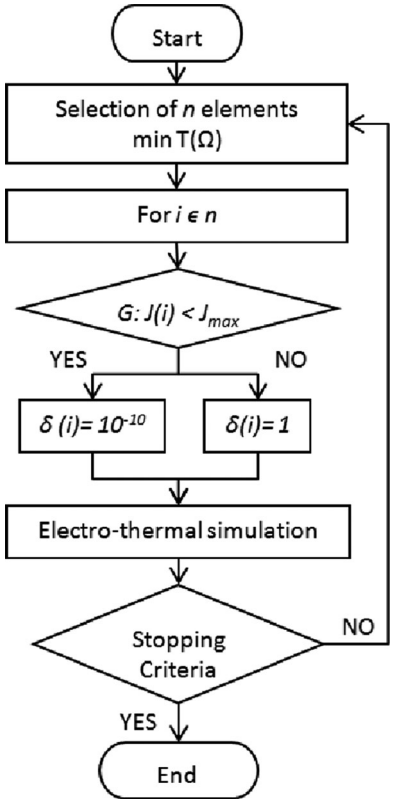

Fig. 10. Flowchart of the algorithm for the extraction of the elements in the busbar 2-D mesh.

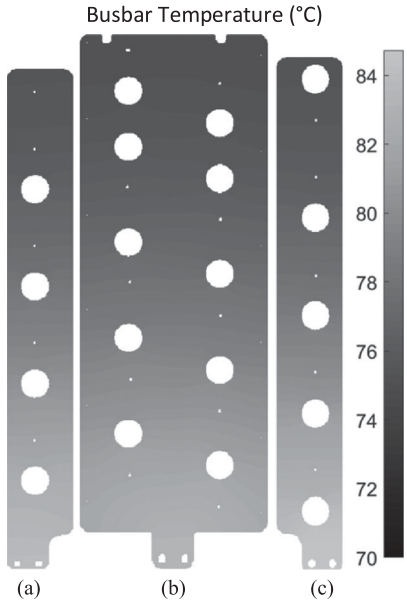

Fig. 11. Temperature distribution in 2-D exploded busbar containing (a) plate 1 (+), (b) plate 2 (MP), and (c) plate 3 (−) side to side.

copper sheets have standard thicknesses, the thickness modification is applied uniformly over the plate. Using the 2-D superposition method, the thickness parameters can be varied without changing the mesh in the geometries.

Then, with the purpose of achieving the temperature limit, the subsequent shape topology optimization is applied in the geometry with the new thickness. The shape topology optimization will proceed by changing the density δ of the elements in the 2-D FEM mesh to reproduce the presence or absence of material. A mapping of the elements' density over the geometry is done, and its values vary in a discrete way. The density is directly related to both conductivities, electrical and thermal, so that a density closer to 0 (to avoid numerical instabilities) equals the absence of material and a density equal to 1 corresponds to the presence of material in the mesh element. This method is coupled with an algorithm (see Fig. 10) that maximizes the energy transfer with the environment and allows the volume minimization of the busbar according to the objective function that depends on the maximum temperature.

The objective function is given by

$$F(\Omega) = T_{\Omega\max} \tag{14}$$

subject to

$$-\nabla \cdot \left(\frac{1}{\rho}(\delta)\nabla V\right) = \nabla J_S \tag{15}$$

$$-\nabla \cdot (\lambda(\delta)\nabla T) + h(T - T_\infty) + \varepsilon\sigma\left(T^4 - T_\infty^4\right) + \frac{\lambda_{12}}{x_{12}}(T - T_2) = \frac{1}{\rho}(\delta)|\nabla V|^2 \tag{16}$$

$$\int_\Omega \delta d\Omega - Vol_0 \leq 0 \tag{17}$$

$$\delta = 10^{-10}, \delta = 1 \tag{18}$$

$$G(J, J_{\max}) = \delta \tag{19}$$

where Ω is the domain of study, meaning all plates of the busbar. Equation (14) stands for the minimization of the domain's volume regarding the maximum temperature. Equations (15) and (16) describe the electrical and the thermal problems, respectively. Equation (16) corresponds to the general thermal equation containing all possible transfers, the equations used are (6), (7), and (8). The minimization of the volume is defined by (17) where the density of some elements δ will be set closer to zero; therefore, the volume will be reduced from the initial volume called Vol_0. In addition, the density of elements δ can only take two values: 1 or 10^{-10} (18). *G* function defined in (19) conditions the value of the element density δ with the value of the element current density J. If the current density of an element is higher than a defined value $J_{\max}$, then its density will not be set close to 0 because it is an important element for the current flow. In this way, *G* function will avoid the creation of domain discontinuities between electrical inputs and outputs.

The algorithm used for the thermal topology optimization finds a local minimum, depending on the initial position (see Fig. 10). In the study case, the busbar initial position is the maximum volume state. The algorithm will target the elements that have a weak energy transfer with the environment. Because of (4), the targeted elements will be the coolest in the domain Ω. So, a group of the *n* coolest elements will be set to density

$\delta = 10^{-10}$ if the function G (19) allows it. Hereafter, a new electrothermal resolution will be solved as the new geometry will modify the current density distribution and, consequently, the temperature. The chosen value for the parameter n must be low, else too many elements could be set to density close to zero compromising the continuity of the electric domain. Setting density δ to 10^{-10} (absence of material) will also modify the thermal transfers between plates and environment. For example, two overlapped plates where before there was conduction (8), in a new state with the absence of material caused by the variation of δ, there will be convection and radiation with the environment (6). This method is iterative until the maximum temperature allowed is reached.

VI. Discussion

The 2-D superposition method can be used to analyze the current density distribution and temperatures in steady state for laminated busbars. The method is validated by an experimental comparison and proves to be a faster method than the 3-D FEM, which is a primordial feature for topology optimization. The implementation of the topology optimization algorithm in the 2-D superposition method provides new geometry shapes while keeping the temperature under the allowed values.

Fig. 11 shows the steady-state temperature at operation conditions with the original geometry simulated in Section IV (1 mm thickness). The hotspots reside in the connecting tabs; the capacitor's connections (small holes) have no thermal effect as the current density is not significant. The highest temperature zone is placed in plate 3 since a large hole next to the connecting tab considerably reduces the current section. The laminated busbar is oversized (temperature $<$ 105 °C), and therefore, optimization can be applied. First, an optimization regarding only the plate's thickness is applied. The thickness is reduced by half (0.5 mm) since copper sheets have standard thicknesses. Because the temperature limit is not yet overcome [see Fig. 14], the shape topology optimization is applied over the geometry with the new thickness. Conductive material is erased by the algorithm (see Fig. 10) assuring the continuity of the domain. The shape modification implies the modification of current flows and, hence, the temperature. The plate 2 (MP) will not take part on the topology optimization because it is used to physically fix the busbar in the converter by its edges. The current density limiting the topology optimization $J_{\max}$ (19) is set to different values in order to compare the different optimization results. The tested values of $J_{\max}$ are integers from 2 to 5 A/mm^2. Because of the presence of lower temperatures, the optimization is first applied in plate 1 (+) and then in plate 3 (−). The geometry evolves forming a new current density distribution where the maximum value in optimized zones is $J_{\max}$. Figs. 12 and 13 show the current density in the original shape but 0.5 mm thickness and the new shapes created by the topology shape optimization according to the $J_{\max}$ value. It can be observed that optimized zones have constant current density $J_{\max}$. In the optimized geometries, black zones with zero current density correspond to empty zones (no material). Regarding the topology optimization results, it is clear that the $J_{\max}$ value is a determinant factor. For a low $J_{\max}$ value (2 A/mm^2), the optimization of plate 1 (+) is quickly limited since the minimal current density exceeds this limiting value. Therefore, optimization continues in plate 3 (−). On the other hand, for high $J_{\max}$ values (5 A/mm^2), plate 1 (+) is highly optimized by creating paths of constant current density value ($J_{\max}$). Consequently, optimization in plate 3 (−) is less significant.

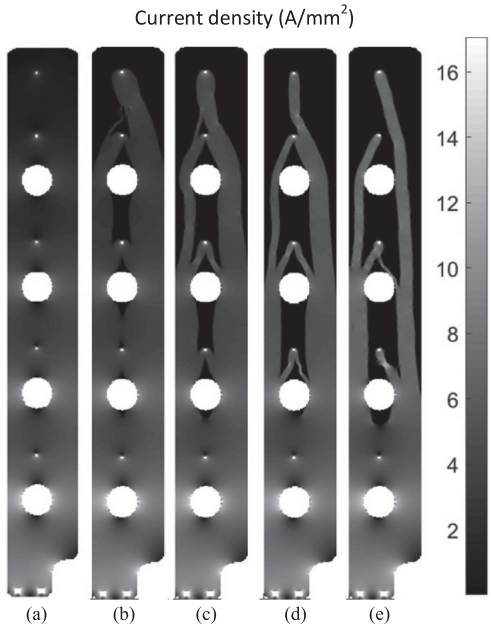

Fig. 12. Current density of plate 1 (+). (a) 0.5 mm thickness original shape. (b) Topology-optimized geometry with $J_{\max} = 2$ A/ mm^2. (c) Topology-optimized geometry with $J_{\max} = 3$ A/mm^2. (d) Topology-optimized geometry with $J_{\max} = 4$ A/mm^2. (e) Topology-optimized geometry with $J_{\max} = 5$ A/mm^2.

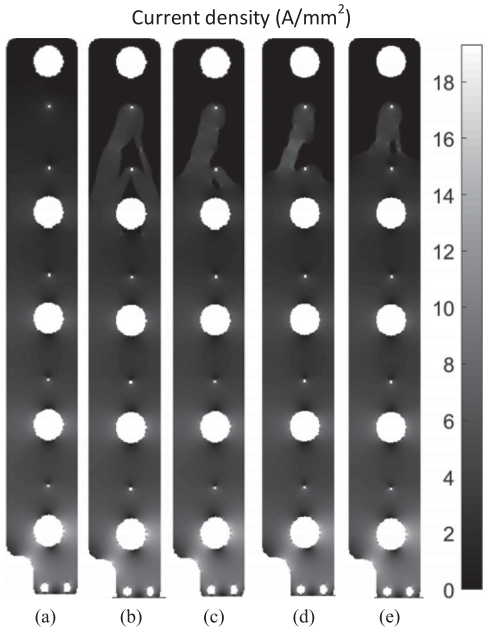

Fig. 13. Current density of plate 3 (−). (a) 0.5 mm thickness original shape. (b) Topology-optimized geometry with $J_{\max} = 2$ A/mm^2. (c) Topology-optimized geometry with $J_{\max} = 3$ A/mm^2. (d) Topology-optimized geometry with $J_{\max} = 4$ A/mm^2. (e) Topology-optimized geometry with $J_{\max} = 5$ A/ mm^2.

Fig. 14 shows the temperature evolution of the optimizations. Original geometry with 1 mm thickness stands for 84.7 °C as

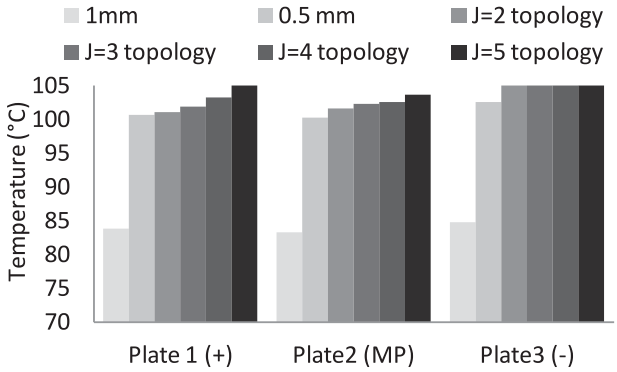

Fig. 14. Maximum temperature of the plates according to the original shape 1 mm thickness, original shape 0.5 mm thickness, and topology-optimized shapes with different $J_{\max}$ criteria and 0.5 mm thickness.

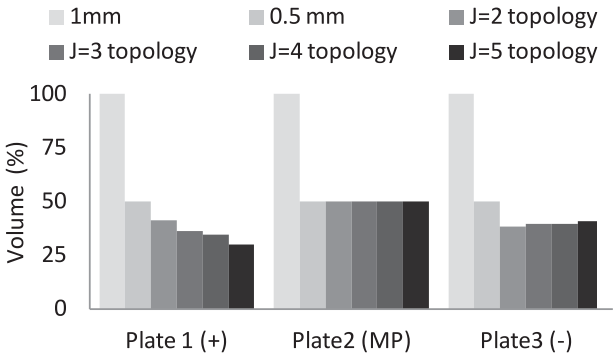

Fig. 15. Comparison of volume minimization in plates between original shape, thickness optimization, and topology optimization with different $J_{\max}$ criteria.

the maximum value, thickness optimization (0.5 mm thickness) rises to 102.6 °C, and the subsequent topology shape optimization of plates 1 (+) and 3 (−) of 0.5 mm thickness reaches the maximum temperature allowed, 105 °C. Fig. 15 compares the resulting volume between plates and optimizations. Optimization in plate 1 (+) has poor effect in the increase of the busbar maximum temperature since plate 2 (MP) works as a heat sink; hence, large amount of material can be economized.

VII. Conclusion

Topology optimization for busbars in power converters is presented. The numerical resolution is performed by the superposition method based in 2-D FEM. This method allows observing current density distributions and steady-state temperatures in a fast way by coupling both 2-D problems: electric and thermal. Thermal transfers between plates depend on their relative position as overlapping determines them. The method is validated by an experimental comparison, which confirms the assumptions in the model. Furthermore, the method shows agreement with the 3-D FEM results and a much more competitive time to results, allowing fast topology optimizations. Finally and taking advantage of the 2-D approach, a thickness and a shape topology optimizations are applied in order to reduce the amount of copper used without exceeding the temperature limits. Shape topology optimization is performed by the defined algorithm and allows a reduction of copper of more than 50% in all tested conditions. However, this topology optimization can deteriorate the inductive effect of the busbar. Future work will include inductance in a multiobjective topology optimization.

References

[1] M. Buschendorf, M. Kobe, R. Alvarez, and S. Bernet, "Comprehensive design of DC busbars for medium voltage applications," in *Proc. 2013 IEEE Energy Convers. Cong. Expo.*, pp. 1880–1885.
[2] H. Wen and W. Xiao, "Design and optimization of laminated busbar to reduce transient voltage spike," in *Proc. 2012 IEEE Int. Symp. Ind. Electron.*, pp. 1478–1483.
[3] D. Cottet, D. Daroui,, and G. Antonini, "EM simulation of planar bus bars in multi-level power converters." presented at the 2012 Int. Symp. on Electromagnetic Compatibility (EMC EUROPE).
[4] J. Hus, "Estimating busbar temperatures," in *Proc. 36th Annu. Petroleum Chem. Ind. Conf. Rec. Ind. Appl. Soc.*, 1989, pp. 119–127.
[5] S. Burtovoy and I. Galkin, "Geometry optimization of half-bridge converter with symmetrical busbar structure," in *Proc. 2012 13th Biennial Baltic Electron. Conf.*, pp. 251–254.
[6] C. Chen, X. Pei, Y. Chen, and Y. Kang, "Investigation, evaluation, and optimization of stray inductance in laminated busbar," *IEEE Trans. Power Electron.*, vol. 29, no. 7, pp. 3679–3693, Jul. 2014.
[7] M. Khan, P. Magne, B. Bilgin, S. Wirasingha, and A. Emadi, "Laminated busbar design criteria in power converters for electrified powertrain applications," in *Proc. 2014 IEEE Transport. Electrification Conf. Expo*, pp. 1–6.
[8] M. C. Caponet, F. Profumo, R. W. De Doncker, and A. Tenconi, "Low stray inductance bus bar design and construction for good EMC performance in power electronic circuits ," *IEEE Trans. Power Electron.*, vol. 17, no. 2, pp. 225–231, Mar. 2002.
[9] B. Eyglunent, *Manuel de Thermique*, 2nd ed. : Paris, France, Hermes Lavoisier.
[10] C. Chen, X. Pei, Y. Shi, X. Lin, X. Liu, and Y. Kang,, "Modeling and optimization of high power inverter three-layer laminated busbar," in *Proc. 2012 IEEE Energy Convers. Cong. Expo.*, pp. 1380–1385.
[11] I. Stevanović, D. Cottet, B. Wider, D. Daroui, and J. Ekman,, "Modeling of large bus bars using PEEC method and circuit level simulators," in *Proc. 2010 IEEE 12th Workshop Control Modeling Power Electron.*, pp. 1–7.
[12] M. P. Bendsøe, "Optimal shape design as a material distribution problem," *Struct. Optim.*, vol. 1, no. 4, pp. 193–202, Dec. 1989.
[13] R. J. Pasterczyk, C. Martin, J.-M. Guichon, and J.-L. Schanen,, "Planar busbar optimization regarding current sharing and stray inductance minimization," in *Proc. 2005 Eur. Conf. Power Electron. Appl.*, 2005, p. 9.
[14] W. Z. Black, "Steady-state and transient ampacity of bus bar," *IEEE Trans. Power Del.*, vol. 9, no. 4, p. 1822–1829, Oct. 1994.
[15] M. Muhammood, M. Kamarol, D. Ishak, and S. Masri, "Temperature rise prediction in 3-phase busbar system at 20 °C ambient temperature," in *Proc. 2012 IEEE Int. Conf. Power Energy*, pp. 736–740.
[16] L. Smirnova, R. Juntunen, K. Murashko, T. Musikka, and J. Pyrhonen, "Thermal analysis of the laminated busbar system of a multilevel converter," *IEEE Trans. Power Electron.*, vol. 31, no. 2, pp. 1479–1488, Feb. 2016.
[17] T. Matsumori, T. Kondoh, A. Kawamoto, and T. Nomura, "Topology optimization for fluid–thermal interaction problems under constant input power," *Struct. Multidisc Optim.,* vol. 47, no. 4, pp. 571–581, Feb. 2013.
[18] A. Iga, S. Nishiwaki, K. Izui, and M. Yoshimura, "Topology optimization for thermal conductors considering design-dependent effects, including heat conduction and convection," *Int. J. Heat Mass Transfer*, vol. 52, no. 11–12, pp. 2721–2732, May 2009.
[19] T. Hong, "Current capability enhancement of bus bars or PCBs by thermal conduction," presented at the PCIM Conf., 2012, Nüremberg, Germany.

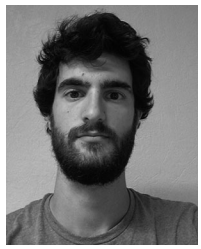

Oriol Puigdellivol received the master's degree in industrial engineering from the Universitat Politècnica de Catalunya (UPC), Barcelona, Spain, in 2013. He is currently working toward the Ph.D. degree in the Laboratory of Power Electronics and Electrical Engineering (L2EP), University Lille 1, Lille, France.

His current research interests include the field of power electronics interconnections.

Damien Méresse received the Ph.D. degree in mechanical engineering from the University of Valenciennes and hainaut-Cambrésis, Valenciennes, France, in 2011.

In 2012, he became Associate Professor in this same university. His current research interests include the inverse heat transfers methods and thermal optimizations.

Yvonnick Le Menach was born in Brittany, France, in 1970. He received the Ph.D. in electrical engineering from the University of Lille, Lille, France in 1999.

From 1999 to 2002, he was an Assistant Professor at the University of Artois, France. Since 2002, he has been an Assistant Professor in the Laboratory of Power Electronics and Electrical Engineering (L2EP), University Lille 1, Lille. His current research interests include the numerical techniques for the finite element method applied to the electromagnetic systems.

Souad Harmand recieved the Ph.D degree in energetics from the University of Valenciennes and Hainaut-Cambrésis (UVHC), Valenciennes, France, in 1990 where she also became Assistant Professor in 1992.

Since 2009 she leads the research group in fluidynamics and thermal transfers (LAMIH UMR CNRS 8201). Since 2014 she is also the Vice-President of the Board of Directors of the UVHC. She has specialized in the thermal transfers by convection on fixed or mobile walls in the presence of complex flows. Her current research interests include the development of new cooling technologies of complex machines, such as heat pipes in alternators or brake discs. She takes part in the activities of the Pole Medee, a research group in electrical machines.

Jean-François Wecxsteen was born in 1964. He received the Civil Eng. degree from Hautes Etudes d'Ingénieur (HEI) de Lille, in 1986.

He is currently with AUXEL-FTG, Gondecourt, France, where he is in charge of the research and development of new technologies in laminated busbars for power converters.